File Name : cms_note.mac.eps
Title : (Adobe Illustrator (R) Version 5.0 Full Prolog)
Creator : Adobe Illustrator(r) 6.0
CreationDate : (3/7/1994) ()

May 1997

Effect of neutron irradiation of MQW lasers to 10^{15}n/cm^2

K. Gill, V. Arbet-Engels, G. Cervelli, R. Grabit, C. Mommaert, G. Stefanini, F. Vasey

CERN, CH-1211, Geneve 23, Switzerland.

J. Troska

Blackett Laboratory, Imperial College, London SW7 2BZ.

Abstract

1300nm edge-emitting multi-quantum-well lasers are the baseline choice for the optical transmitter in the CMS tracker optical links. The radiation environment is expected to be ~10Mrad and ~10^{14}(neutron-equivalent)/cm^2 over ten years. Lasers from four manufacturers have been irradiated in naked die form with neutron fluences of ~$2x10^{14}$n/cm^2. One laser type was also irradiated in a fully packaged, fibre-pigtailed form up to ~10^{15}n/cm^2. Neutron damage caused an increase in laser threshold current and a decrease in output efficiency, but little change in signal-to-noise ratio, linearity, and emission wavelength spectrum.

1. Introduction

All of the optical link components situated inside the CMS tracker must be both sufficiently reliable and radiation resistant to last ten years of operation. At 20cm from the beam axis, radiation levels are expected[1] to be ~10Mrad and ~10^{14}(neutron equivalent)/cm^2. The optical link transmitter elements are considered to be the most critical component in terms of radiation resistance and reliability since they are located inside the tracker volume. Induced radioactivity inside the experiment, plus the overall complexity of the apparatus, will not permit extensive maintenance, or replacement, of the optical link components. Previous irradiation studies[2], in conjunction with other criteria such as cost, and future component availability, led to the decision[3] to base the optical links on directly-modulated, 1300nm edge-emitting, multi-quantum-well (MQW) lasers[4]. Results are presented for the effect of neutron damage on the characteristics of several types of 1300nm MQW lasers. This investigation forms part of an on-going series of radiation damage and reliability studies of lasers for the CMS tracker optical link.

1.1 MQW Lasers and radiation damage effects

All of the devices tested are based on a strained InGaAsP MQW active volume, epitaxially grown onto an InP substrate. The proportions of the constituent elements in the $In_{1-x}Ga_xAs_yP_{1-y}$ growth fix the band-gap in the quantum well and barrier layers and strain is introduced by the slight mismatch in lattice constants. The band-gap and the thickness of the quantum wells determine the laser wavelength. Quantum wells increase the confinement of injected carriers to the active region, resulting in a lower threshold current than in conventional heterostructure lasers.

Up to the laser threshold current there is no optical gain and the devices behave like LEDs, with spontaneous recombination of electrons and holes resulting in light emission. Stimulated emission can occur but more photons are absorbed, or lost from the cavity, than are created. At the threshold current more photons are created than are absorbed or lost; the cavity becomes transparent and optical gain occurs, causing an increase of (coherent) light output by several orders of magnitude. Above threshold, the laser operates in a linear region with practically 100% of the injected current being converted into light.

In semiconductors, the displacement of atoms from their lattice sites by radiation damage introduces defects that can act as recombination centres[5]. Figure 1 illustrates how defect-related recombination centres can interfere with the laser operation. Below threshold, recombination at the defect states competes with radiative transitions and drains the injected

charge carriers at some rate[6]. A higher injected current level is therefore required for transparency, causing the observed increase in threshold current[6-10]. Above threshold, the stimulated recombination lifetime is much shorter than the lifetime related to recombination at the radiation induced defects and the laser slope-efficiency above threshold (dL/dI, where L is the output light power at current I) is therefore relatively unaffected by radiation damage[6-10]. Degradation of the laser packaging by radiation damage can, however, cause significant attenuation of the output power[9]. The emission spectrum of semiconductor lasers is found to be unaffected by radiation damage[7]; this should also be the case in MQW lasers providing the physical integrity of the strained quantum-well structures is not affected by radiation damage.
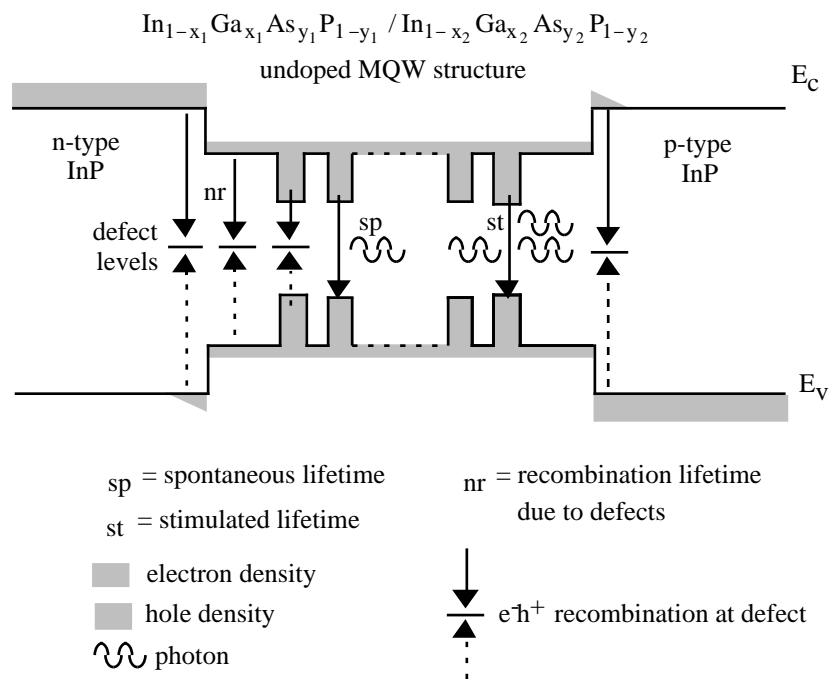

Figure 1: Schematic energy gap diagram of a forward biased InGaAsP/InP MQW laser showing spontaneous, stimulated, and defect-induced electron-hole recombination.

2. Experiment

2.1. Devices

Lasers from four manufacturers (labelled A, L, M and N) were tested in the form of naked die mounted in transistor-outline (TO) cans. Table 1 shows the number of devices measured and irradiated in this investigation. The lasers were all edge-emitting with a peak wavelength

~1310nm and narrow spectral width. In this study, Type N lasers were also evaluated in a fully packaged form (labelled as Type NP) with the lasers mounted on silicon substrates pigtailed with single-mode fibre and housed in an 8-pin DIL package. The fibres are actively aligned before being soldered into place. By testing naked die (in TO-cans), the radiation hardness of the actual laser chip can be determined. Evaluation of type N lasers in both naked and fully packaged form allows radiation damage effects, at both device and package level, to be distinguished.

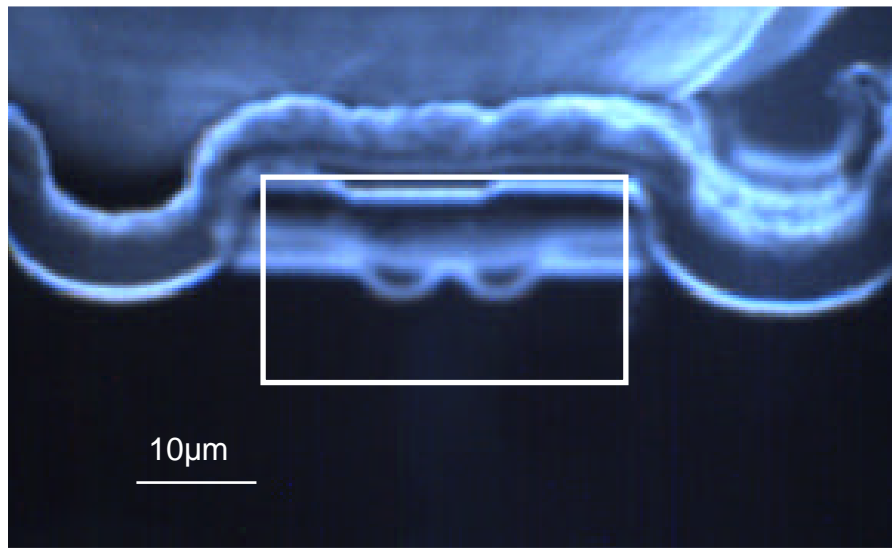| Laser type	A (TO-can)	L (TO-can)	M (TO-can)	N (TO-can)	NP (Type N in 8-pin DIL)
No. tested	2	3	3	5	10
No. irradiated	2	2	2	4	5

Table 1: Number of each type of laser tested and irradiated.

More information was available on Type N devices, which make up the bulk of the lasers under test. These lasers are based on a double channel planar buried heterostructure (DCPBH)[4] geometry. Figure 2(a) shows the cleaved facet of a Type N laser, using a scanning electron microscope (SEM) image combined with an electron beam induced current (EBIC)[11] measurement; figure 2(b) illustrates the active region in greater detail. The die size is $200 \times 100 \times 300 \mu m^3$ (width x height x [cavity] length) and the active region has a cross-sectional area of approximately 1.5μm x 150Å. The EBIC scan shows the location of p-n junctions making the two confinement channels visible; these p-n-p-n structures confine the injected current to the active laser volume resulting in a low threshold current (~10mA). The two larger etched trenches isolate the laser from the rest of the die.
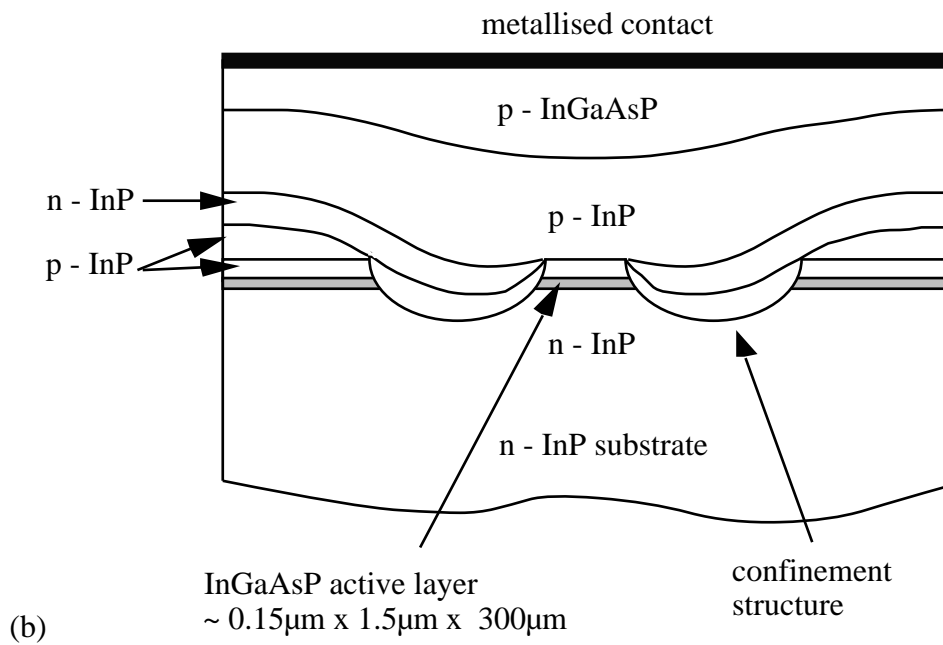
2.2 Measurements

2.2.1 L-I characteristics

The output power versus input current characteristics (L-I curve) were measured in the lab for each laser, before and after irradiation, with the arrangement shown in Figure **3**. For the naked lasers, a large area germanium photodiode (ø=5mm) was used to collect all of the light, which is typically emitted in an elliptical cone with a maximum FWHM angle of ~30°. The fully packaged lasers were measured using the same set-up but with a fibre-pigtailed InGaAs p-i-n detector.

(a)

metallised contact

p - InGaAsP

n - InP

p - InP

p - InP

n - InP

n - InP substrate

InGaAsP active layer
~ 0.15μm x 1.5μm x 300μm

confinement
structure

(b)

Figure 2: (a) SEM/EBIC image of Type N laser[11] and (b) schematic cross-section of a DCPBH laser[4] which describes the region framed in fig 2(a).
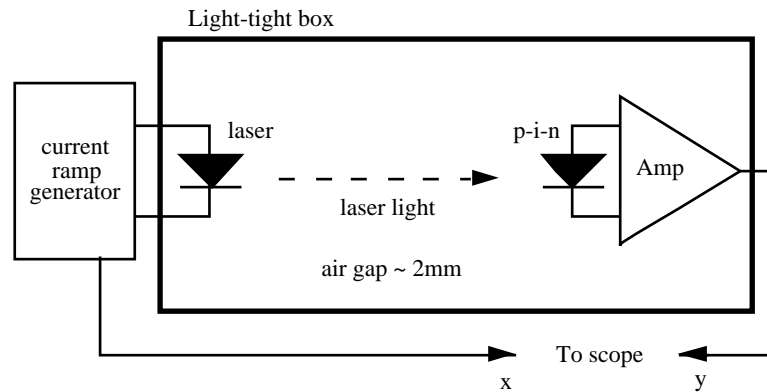
Figure 3: Lab set-up for laser L-I characteristic measurement

The laser threshold and laser slope-efficiency (dL/dI) can be determined from the L-I characteristics. The threshold sets a lower limit on the d.c. operating point of an analogue transmitter and the slope-efficiency determines the gain required in the laser driver for a certain range of output optical power. The laser threshold was defined as the intercept (at the current axis) of a line fitted to the L-I data above the threshold[12], after subtracting any d.c. offset at zero input. The slope-efficiency was defined as the gradient of this fitted line.

2.2.2 Linearity

For a robust analogue readout system, deviations from linearity above threshold should be minimal. If the L-I transfer characteristic is non-linear, but monotonic and stable in time, it is possible to calibrate the system to correct the non-linearity. For our proposed 50000 channel system it is clearly advantageous to select a laser that has sufficiently linear performance. The optical link specifications are not yet finalised but the maximum deviation from linearity for the whole link is anticipated to be <2%[13]. The linearity of each laser under test was determined by measuring the deviation from a second line, fitted to the L-I data over a certain power range[12]. Non-linearities in the laser driver and the receiver (and amplifier) were investigated separately and found to be at a negligible level.

2.2.3 Signal to noise performance

To transfer analogue signals from the front-end readout chips[14] over the range of several minimum-ionising particles (MIPs) without significant distortion, a dynamic range of 7-8 bits is specified for the CMS tracker optical link[13]. Ideally, the noise level in the system should be less than one third of the least significant bit. Using a low noise (~50ppm) d.c. current source, a small p-i-n photodiode (ø=300μm) for the naked lasers, and a fibre-pigtailed

InGaAs p-i-n photodiode for the packaged (Type NP) lasers, the noise of each laser was measured at several points along the L-I curve. The noise was calculated as the r.m.s. value of the a.c. coupled output signal. The bandwidth of the measurement was 10Hz-30MHz and the noise due to the oscilloscope, photodiode and output amplifier was subtracted by using measurements below the laser threshold.

2.3. Irradiation conditions

The devices were irradiated with neutrons (~6MeV) at the SARA facility[15] in Grenoble. Figure 4 illustrates the experimental arrangement. The naked lasers were arranged in front of the beryllium target; their output power was monitored by 2mm diameter InGaAs p-i-n photodiodes (a primary detector and two back-up devices). The p-i-n detectors were situated behind the source at the end of a 1m tube, in a polyethylene box to attenuate the neutron flux incident on the detectors and readout electronics. The packaged lasers were connected via a polyethylene shielded optical fan-in to an 8-way fibre ribbon that transferred the signals to pigtailed InGaAs p-i-n detectors located in the control room. The temperature in the source cell and control room was monitored but not controlled; it was around 18°C during the test with ±2°C maximum fluctuations in the source cell, and 18±4°C in the control room.
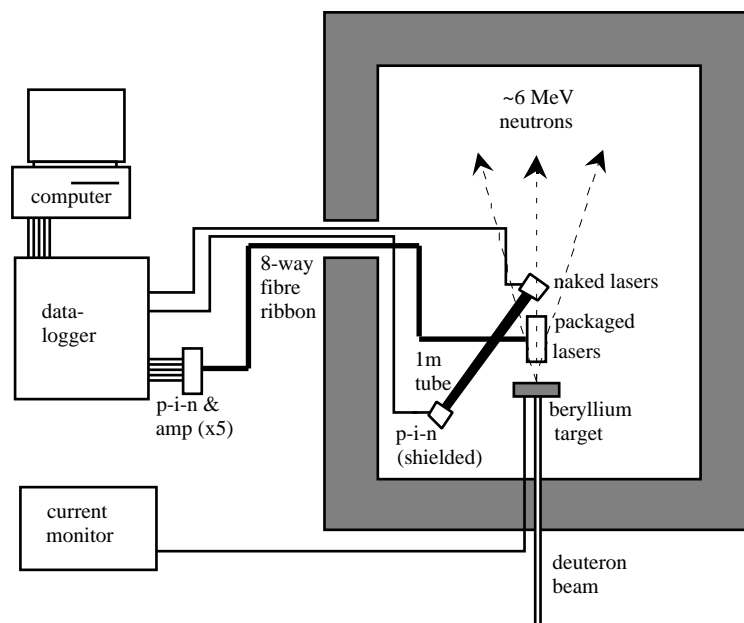

Figure **4**: Schematic arrangement of samples in the irradiation cell

The neutron fluence was measured by activated foil dosimetry (using 4mm diameter foils) with the different fluences given in Table 2. The absolute accuracy is ~15% due to uncertainty in activation cross-sections, but results are typically reproducible to within a few percent. A dosimetry foil was affixed to each Type NP device and one foil was used per pair of naked lasers. By measuring the integrated beam current, the time-stability of the neutron source was checked at 30 minute intervals during the irradiation; the current was roughly constant over the irradiation period of approximately 102 hours.

The devices were monitored for ~100 hours before irradiation, 102 hours during the irradiation, and a further 1500 hours (~2 months) after irradiation to measure any annealing. Measurements were performed in a cycle typically 40 minutes in duration. A cycle was necessary in order to measure the naked lasers individually with the same p-i-n detector. The first ten minutes of each cycle were used to measure the laser L-I characteristics. Between 20 and 50 points were measured per L-I curve; each data value was the average of 5 measurements (total time <1s) after allowing 1s of settling time. Five minutes were then required to monitor p-i-n devices also being evaluated[16]. For the remainder of the cycle, ~25 minutes in the 40 minute period, all the lasers were biased a few milliamperes above threshold to simulate realistic operating conditions. In order to track the threshold changes due to radiation damage, it was necessary to change the current range of the L-I measurements, in addition to the d.c. current value in the last part of the cycle. To reduce the data volume, the cycle duration was increased to one hour during the first week of annealing, and subsequently to two hours.

device(s)	neutron fluence $(\times 10^{14} n/cm^2)$ $\langle E \rangle = 6MeV$	device(s)	neutron fluence $(\times 10^{14} n/cm^2)$
laser NP 1	8.5	2 Type N lasers	1.6
laser NP 2	6.7	(TO-can, biased)	
laser NP 3	5.5	2 Type M lasers	1.7
laser NP 4	4.4	(TO-can, biased)	
laser NP 5	3.5	2 Type A lasers	1.6
2 Type N lasers	3.4	(TO-can, biased)	
(TO-can, unbiased)		2 Type L lasers	2.1
		(TO-can, biased)	

Table 2: Neutron fluences received by the different lasers.

3. Results

3.1 Lab measurements before irradiation

3.1.1 L-I characteristics

Figure 5 shows the L-I curves measured in the lab before irradiation for the naked lasers and packaged lasers respectively. The naked lasers have a range of threshold currents, between 6 and 10mA, and slope-efficiency values between 0.40 and 0.58W/A. There is a systematic uncertainty of ~15% in the slope-efficiency for the naked lasers due to the uncertainty in the p-i-n responsivity. For the fully packaged lasers, the threshold currents are in the range of 8 to 10mA and the slope-efficiencies are between 0.12 and 0.29W/A. The efficiencies are lower for the packaged lasers as only a fraction of the laser light is coupled into the single-mode fibre. The large spread in efficiency values for the packaged lasers results from different levels of laser-fibre coupling, probably due to mechanical alignment effects and different lens quality at the laser-end of the fibre pigtail.
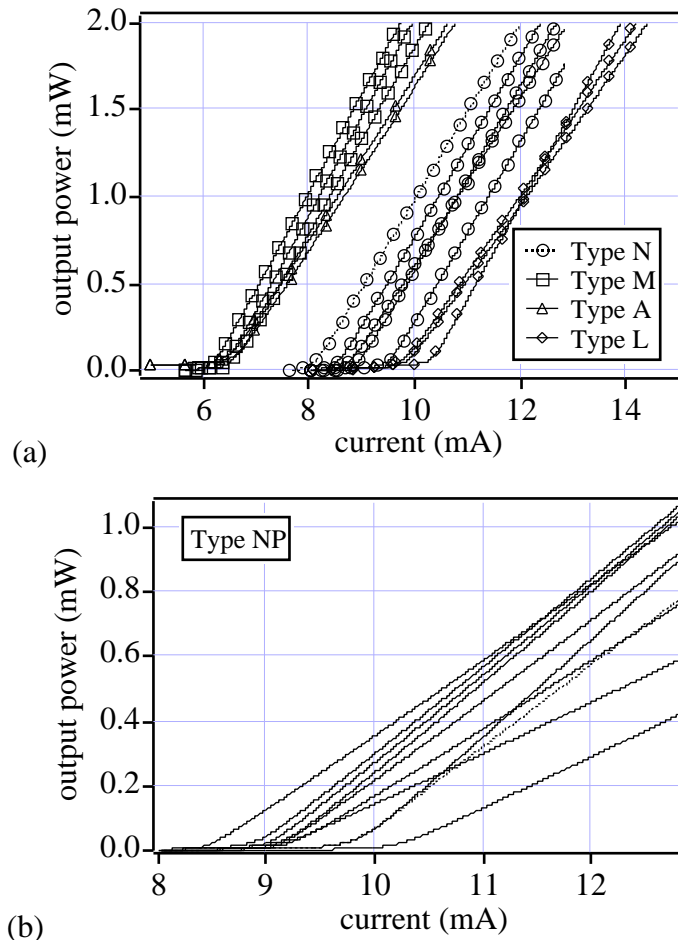
(a)

(b)

Figure 5: Laser L-I curves measured before irradiation for (a) all the naked lasers, and (b) for fibre pigtailed, fully packaged Type NP devices.

3.1.2 Linearity

The deviation of the L-I curves from linearity before irradiation is shown in figure 6 for Type N and NP lasers. Similar results were obtained for the other laser types. A smaller power range is used for the fully packaged lasers since the laser-fibre coupling efficiency is approximately one third that of the naked lasers coupled into the large (ø=5mm) p-i-n diode. An analogue range equivalent to 4MIPs in the final system[13] is illustrated along with the data.
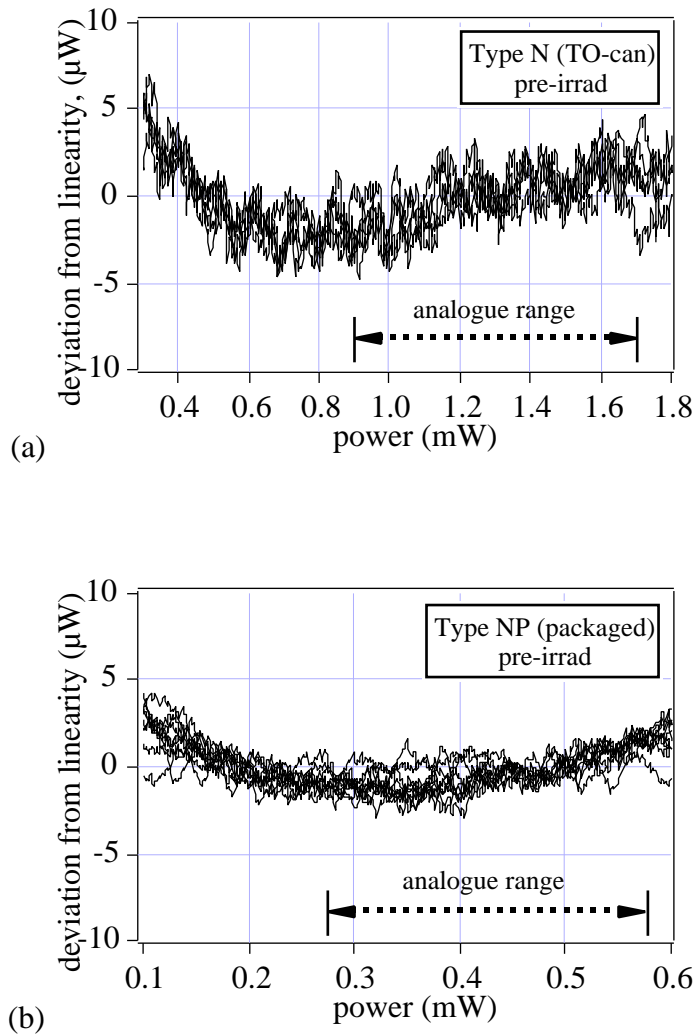

(a)

(b)

Figure **6**: Linearity results for type N and NP lasers before irradiation. An analogue range equivalent to 4MIPs in the final system is also shown.

3.2 Measurements during irradiation and recovery period

3.2.1 Threshold changes

The threshold current with time is shown in figures 7 and 8 for the naked and packaged lasers respectively (part (a) shows the results from -25<t<125 hours and (b) shows the whole data set). Irradiation took place between t=0 to t=102.5 hours. The threshold appears to increase roughly in proportion to the neutron fluence, followed by a recovery of ~30% of the threshold shift in the two month period following irradiation. A power cut occurred during the period 503<t<600 hours during which time the lasers were unbiased and no data was recorded. The recovery of the threshold damage appears to have been suppressed during the power cut. We plan to investigate this effect in more detail in future tests but it is consistent with evidence of enhanced annealing by increased current in irradiated lasers[8] and LEDs[17].
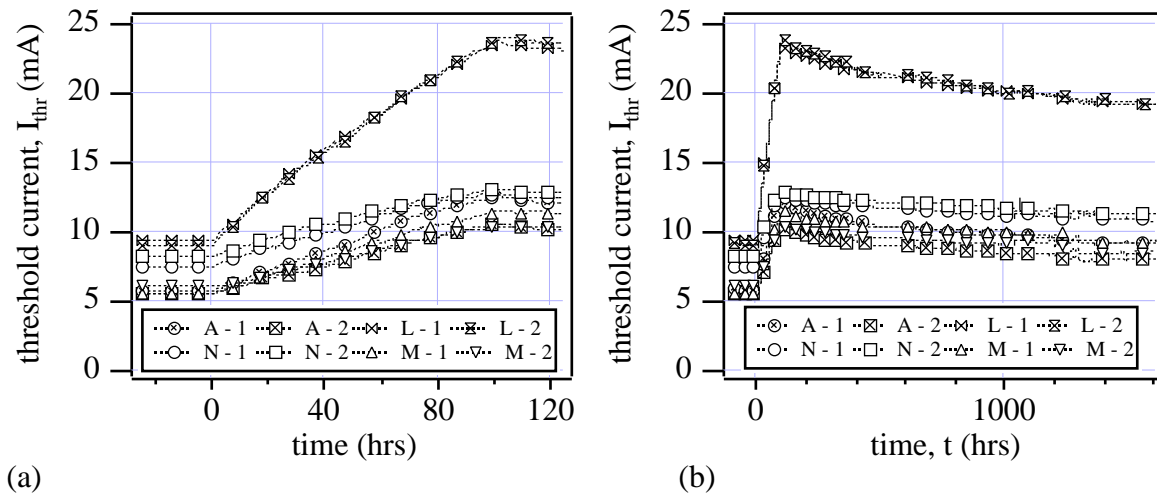
(a)   (b)

Figure 7: Radiation induced threshold current changes in naked lasers.

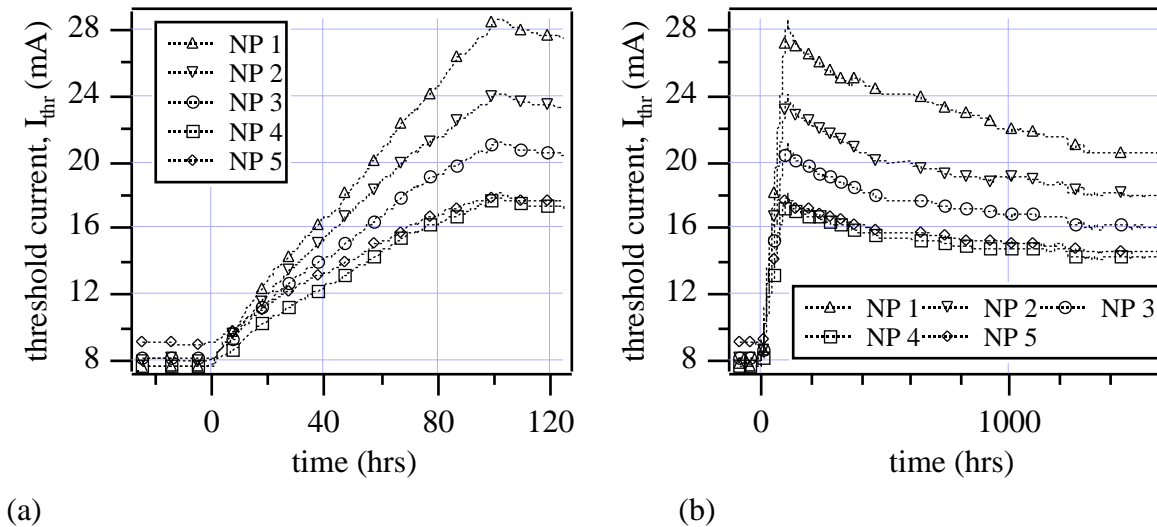(a)   (b)

Figure 8: Radiation induced threshold current changes for packaged lasers.

The threshold shifts are plotted as a function of neutron fluence in figure **9**. For the naked lasers of the same type, the results do not completely agree in all cases probably because of uncertainties in the actual fluence at each laser (one dosimetry foil was placed between each set of two naked lasers of the same type). For the fully packaged Type N lasers the dosimetry was more accurate (one foil per device) and there is a clear agreement between the results for each laser. There is also good agreement between the results for the naked Type N lasers and the fully packaged Type NP devices. A slight decrease in the rate of threshold current change with fluence is observed for each fully packaged device; this behaviour is consistent with annealing taking place during the irradiation and a correction for this dose-rate effect is proposed in Section 4.
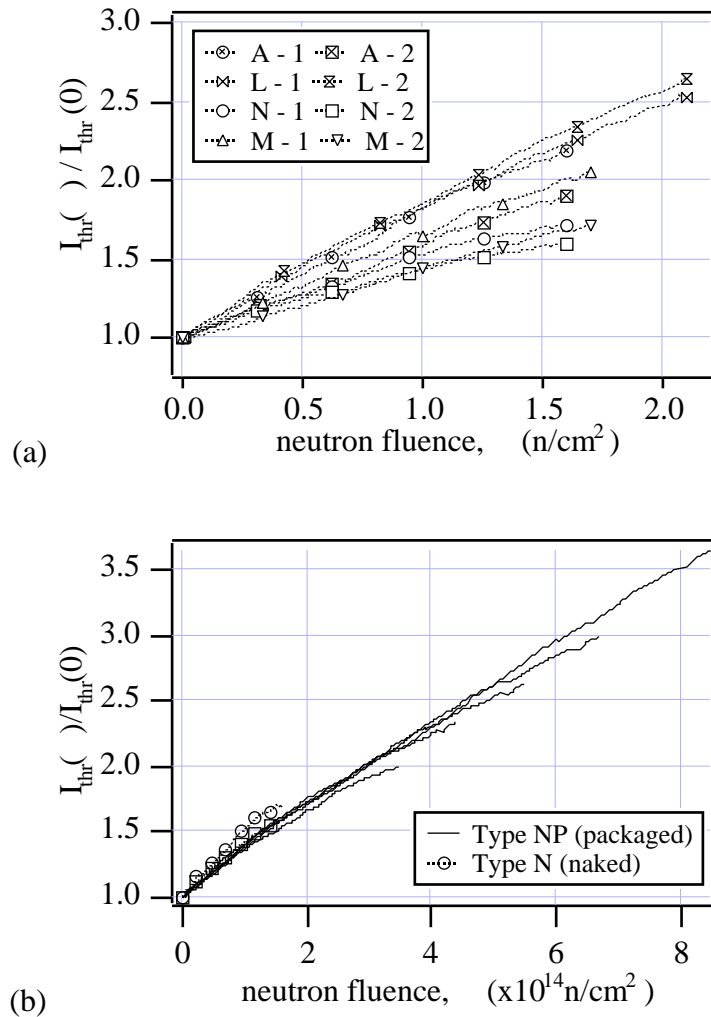
(a)

(b)

Figure 9: Relative threshold current change versus neutron fluence for (a) naked lasers and (b) fully packaged Type NP (and naked Type N) lasers.

3.2.2 Efficiency loss

The laser slope-efficiency, determined from a fit to the data points above threshold, is shown as a function of time in figures 10 and 11 for the naked and packaged lasers respectively. Note that the full data set is limited to t<360 hours as the devices had to be moved in order to retrieve the dosimetry foils. This movement disturbed the amount of light coupling between each laser and the monitoring p-i-n detector. For t>360 hours the threshold values of the lasers could still be determined but the efficiency could not be reliably related to the pre-irradiation value.

All of the naked lasers have a fast decrease in efficiency of ~13%, over the first few hours, followed by a roughly linear change during the rest of the irradiation period (up to t=102.5hrs). Although there is some annealing of the efficiency damage in the period following irradiation, it is clear from the results that the bulk of the apparent efficiency loss (most likely related to the fast damage component) does not anneal. Results of lab measurements of the slope-efficiency after irradiation for the naked lasers are shown in Table 3. As seen in a previous study[2], there is relatively little change in the slope-efficiency before and after irradiation; the fast decrease in efficiency is therefore attributed to radiation damage of the monitoring photodiodes rather than the lasers.

device (Type & No.)	n-fluence 10^{14}n/cm^2 <E>=6MeV	E pre-irrad (±0.01W/A)	E post-irrad (±0.01W/A)
N 6	1.6	0.51	0.51
N 7	1.6	0.53	0.53
N 8 (unbiased)	3.4	0.52	0.50
N 9 (unbiased)	3.4	0.48	0.48
M 1	1.7	0.56	0.53
M 2	1.7	0.56	0.55
A 1	1.6	0.48	0.46
A 2	1.6	0.48	0.46
L 1	2.1	0.55	0.58
L 2	2.1	0.43	0.43

Table 3: Slope efficiency results before and after irradiation from lab L-I measurements of naked lasers.
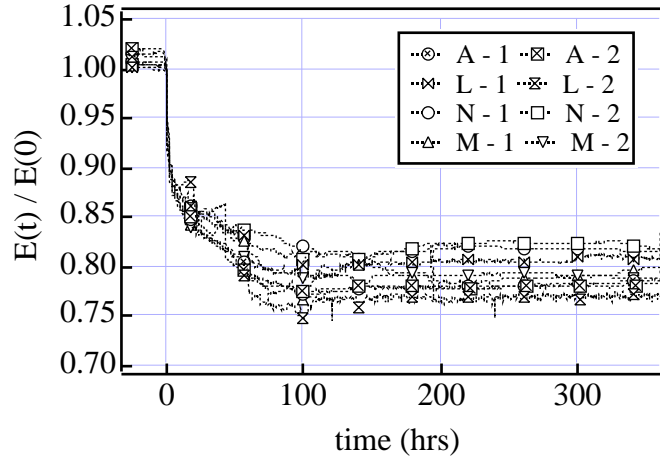
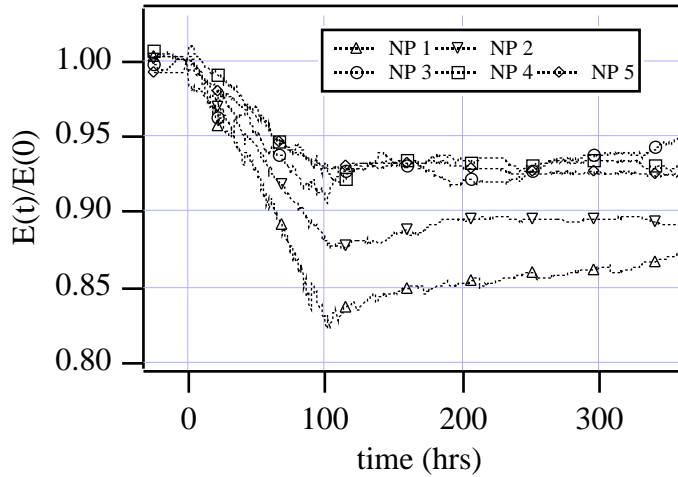Figure 10: Radiation induced change in slope-efficiency for naked lasers

Figure 11: Radiation induced change in slope-efficiency for packaged lasers

For the packaged Type NP devices, a roughly linear decrease in slope-efficiency with fluence is observed as in Figure 12. A ~2% loss of slope-efficiency per 10^{14}n/cm^2 is observed, in reasonable agreement with the ~5% loss in the linear part of the results for the naked Type N lasers. To confirm that these losses are really due to radiation damage of the laser rather than, for example, attenuation in the germanium-doped fibre pigtail, we plan to irradiate some more naked Type N lasers in TO-cans to ~10^{15}n/cm^2. Future tests on packaged lasers will also use radiation resistant[18] pure-silica core fibre pigtails.
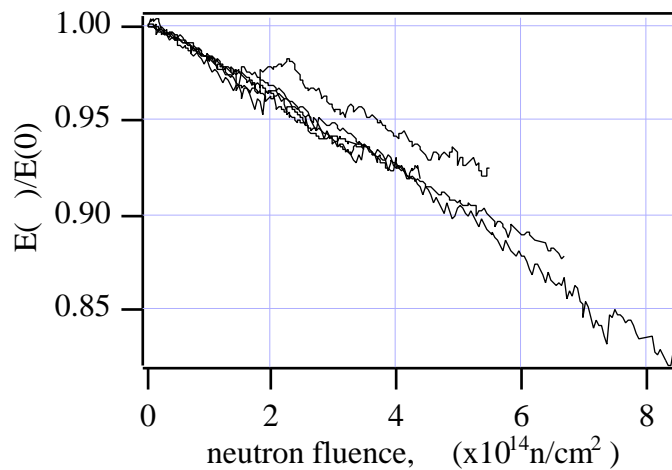
Figure 12: Change in laser slope-efficiency for packaged
Type NP lasers versus neutron fluence

3.3 Lab measurements after irradiation

3.3.1 Linearity

From the L-I curves measured in the laboratory after irradiation, the linearity of the transfer characteristic of each laser was determined. Results are shown in Figure 13 for naked Type N lasers and fully packaged Type NP lasers (to be compared with the pre-irradiation results in Figure 6). Overall the deviation from linearity is not significantly affected by irradiation, and is still <1% (deviation divided by the power interval). The other naked laser types also had very little change in the deviation from linearity after irradiation.
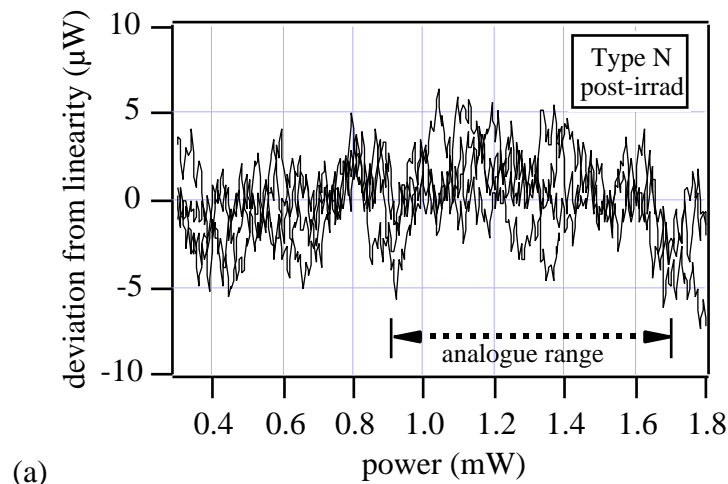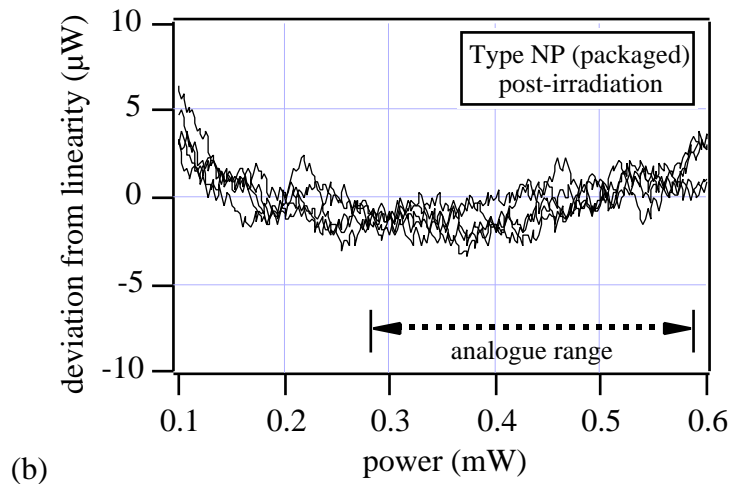

(a)

Figure **13**: Linearity results after irradiation for (a) Type N naked lasers, and (b) Type NP packaged lasers. An analogue range equivalent to 4MIPs in the final system is also shown.

3.3.2 Signal to noise performance

The signal to noise results measured after irradiation are shown in figure 14 for Type N and NP lasers. Due to time constraints, measurements were not carried out before irradiation; however, there were a sufficient number of similar, unirradiated Type N (and NP) lasers to make a reasonable comparison of irradiated and undamaged lasers.

The signal to noise ratio in the naked lasers was not affected by neutron irradiation (similar results were obtained for all the naked lasers), but the signal to noise ratio in the irradiated packaged lasers was a factor ~2 lower than in unirradiated devices. These devices received a much larger neutron fluence than the naked lasers but, as there is no clear dependence on neutron fluence, the cause of the decrease is unknown.

3.3.3 Laser spectrum[19]

The spectrum of each packaged Type NP laser was measured before irradiation by the supplier. After irradiation, four of the irradiated Type NP lasers were remeasured in addition to two of the unirradiated devices, to check the reproducibility of pre-irradiation measurements. No significant differences were found in the spectra measured before and after irradiation.
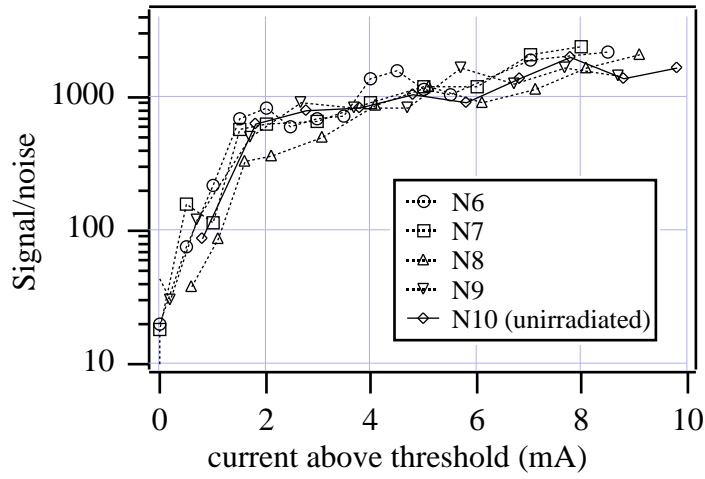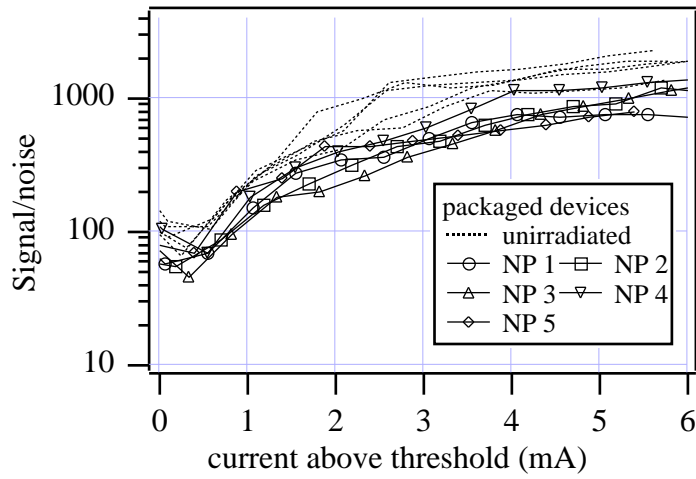
Figure 14: Laser signal to noise measurements with irradiated lasers compared to unirradiated devices for (a) naked Type N, and (b) for packaged Type NP lasers.

4. Estimate of neutron induced threshold shift at the LHC

The increase in laser threshold after irradiation means that the laser driver chip must be able to track the changes in threshold to maintain the same range of optical power output. As the neutron fluences were obtained over the period of several days, rather than years as in the real application, the changes in the threshold current during LHC operation will be different to those presented here due to dose-rate effects. It is therefore useful to develop a model to predict the change in laser threshold due to irradiation with an LHC neutron flux profile.

The threshold damage results are similar to the linear build-up and exponential recovery of the leakage current observed in irradiated silicon detectors[20], where the following empirical parameterisation is applied:

$$\text{during irradiation } (0<t<T): \quad I = \sum_i \frac{\alpha_i \phi}{T}(1 - e^{-t/\tau_i}) \tag{1}$$

$$\text{after irradiation } (t>T): \quad I = \sum_i \frac{\alpha_i \phi}{T}(1 - e^{-T/\tau_i})e^{-(t-T)/\tau_i} \tag{2}$$

where ϕ is the neutron fluence, t is time and T is the duration of the irradiation (assuming a uniform flux). The whole set of data for the five irradiated lasers was fitted with one set of damage constants α_i and recovery time constants τ_i. Several components were required for the best fit. The results of the fit are shown in figure 15 with the values for α_i and τ_i in Table 4. The data taken during the time (503<t<600 hrs) when the power to the lasers was off (and recovery suppressed) have been removed from the fit.

i	α_i [mA/(n/cm^2)]	τ_i [s]
1	1.6±0.1 x10^{-14}	44±2 x10^3
2	6.5±0.7 x10^{-15}	1.42±0.08 x10^6
3	1.8±0.2 x10^{-14}	3.0±0.3 x10^7

Table 4: Fitted constants for threshold current change during and after irradiation

Although the fitted curves describe the overall results fairly well, it is optimistic to base a model on these fit parameters since the largest time constant is several times longer than the period of time over which the results were acquired. Ideally the laser recovery should have been observed (under bias) for ~1 year to constrain the fit more tightly. For practical reasons

it may be sufficient to monitor the annealing rates at different elevated temperatures in order to predict the recovery time constants at room temperature; this procedure will be included in our next irradiation test. In the meantime, an estimate of the threshold current increase at the LHC can be made using the results in Table 4, in addition to a more conservative, worst-case approach using another fit to the data with the longest time constant set as $\tau_3 = \infty$, such that the defects producing this part of the threshold shift do not anneal.
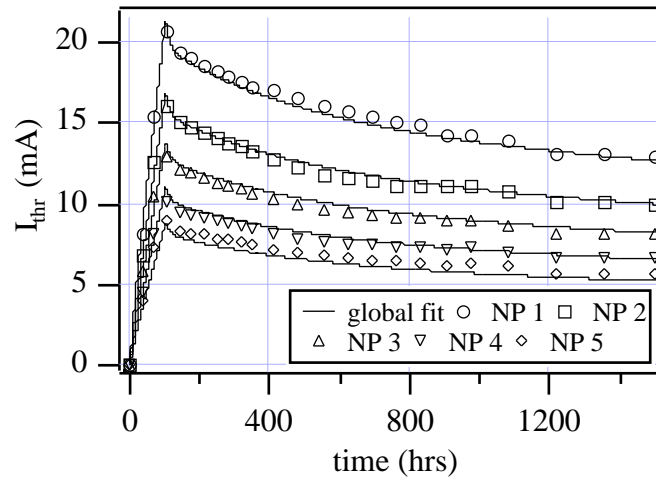
Figure 15: Global fit to the laser threshold current changes for packaged Type NP devices.

A neutron equivalent (n-eq) flux profile of 5×10^{14}(n-eq)/cm^2 over 10 years was simulated, with six months beam-on, six months beam-off in each annual cycle. The n-equivalent flux assumes that the relative damage of charged hadrons, mainly protons and pions, is equal to that due to neutrons. The estimated threshold shifts are shown in Figure 16 for three different 10 year (high LHC luminosity) predictions: (a) using the results in Table 4, assuming the lasers to be continuously biased; (b) using the same results as (a) but with lasers switched off, which is assumed to supress annealing during the LHC beam-off periods (consistent with the results, where no annealing occured during the four day power cut); and (c) using the results of the second fit with $\tau_3 = \infty$.

For prediction (a), the laser threshold current increase is estimated to be less than ~1.2mA. If electrical bias is not applied during beam-off periods, as in case (b), the maximum threshold change increases to ~2mA. In the worst-case, prediction (c), the threshold current change is estimated to increase by ~1.4mA per 10^{14}(n-eq)/cm^2. In both (a) and (b) the current component with the longest time constant (~3×10^7s) is responsible for almost all of the threshold current change over the ten year operational period; the components with shorter time constants saturate quickly at less than 0.1mA.

These estimates apply only to Type N (or NP) lasers and no correction was made for the difference between the neutron spectra of the SARA source[15] and that of the n-equivalent energy spectrum inside the CMS tracker. However, the main assumption is probably that incident charged hadrons cause the same amount of damage as neutrons. If the damage constants $_i$ are determined by the non-ionising energy loss (NIEL)[21] of the incident radiation, it should be possible to calculate the displacement damage due to charged hadrons more accurately.
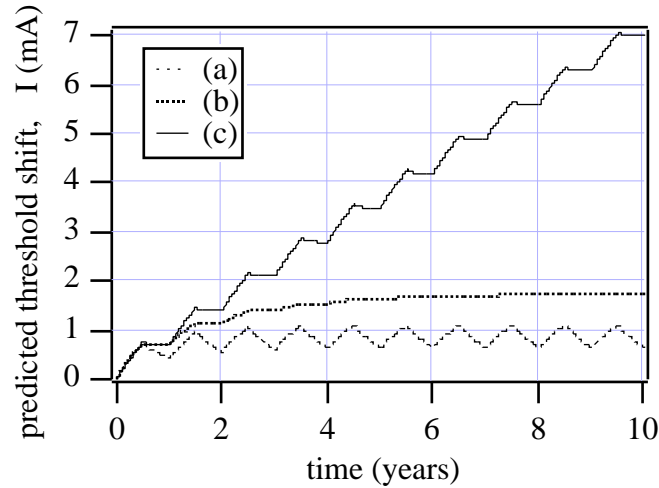

Figure 16: Estimated laser threshold current changes for the CMS tracker for the three cases (a), (b) and (c) outlined in the text, assuming a fluence of 5×10^{13}(eq-n)/cm^2 each year.

5. Conclusions

1300nm, edge-emitting, MQW lasers from four manufacturers have been irradiated, in naked die form, with ~6MeV neutrons up to a fluence of ~2×10^{14}n/cm^2. Other samples of Type N lasers (labelled as Type NP) were also irradiated in a fully packaged, fibre-pigtailed form, with fluences up to 8.5×10^{14}n/cm^2.

The laser threshold current increases with neutron fluence and there is some recovery of the damage during and after the irradiation. The amount of radiation induced threshold shift therefore depends upon both neutron flux, total fluence, and recovery time. The observed damage in the fully packaged lasers was parameterised with a simple model and the effect of a neutron flux profile, similar to that expected in the CMS tracker, was estimated. In the most conservative estimation based on the fitted results, the laser threshold (in Type N or NP devices) will increase by 1.4mA per 10^{14}n/cm^2.

The laser slope efficiency is also affected by neutron damage changes, but to a smaller extent than the threshold change. A decrease of slope-efficiency of ~2% per 10^{14}n/cm^2 was measured for the fully packaged Type NP lasers. There was also some recovery of the damage but the measurements were too noisy to fit the data with the same model used for the threshold shifts. Larger efficiency losses (~20%) were observed during irradiation for the naked lasers but these extra losses were attributed to damage of the monitoring photodiodes rather than the lasers.

The deviation from linearity of the laser output characteristics was found to be <1% over a realistic power window and the linearity was unaffected by irradiation. The signal to noise performance of the lasers is capable of supporting the 7-8 bit dynamic range of our proposed system before and after irradiation. The spectrum of the fully packaged lasers was also unaffected by radiation damage.

Further irradiation tests are planned in 1997 to confirm these results and to evaluate the radiation resistance of the lasers to gamma and proton damage. An experiment is also planned to determine the time-to-failure of irradiated lasers as no data exists for the reliability after irradiation for the tested laser types.

Acknowledgements

References

[1] The Compact Muon Solenoid Technical Proposal. CERN Report LHCC 94-38 (1994).
[2] "Neutron damage studies of semiconductor lasers for the CMS tracker optical data links", K. Gill et al. Proceedings of Second Workshop on Electronics for LHC Experiments, Sept. 1996. (also available as CMS Technical Note 96-014).
[3] "Fibre optic link technology for the CMS tracker", G. Hall, G. Stefanini and F. Vasey, CERN CMS Note 1996/012.
[4] "Semiconductor lasers", 2nd Edition, p. 202, G. P. Agrawal and N. K. Dutta. Van Nostrand Reinhold, New York (1993).
[5] "Basic radiation effects in nuclear power electronics technology", J. E. Gover et al., Sandia Laboratory Report, SAND85-0776 (1985).

[6] "Radiation effects in optoelectronic devices", C. E. Barnes and J. J. Wiczer, Sandia Laboratory Report, SAND84-0771 (1984).

[7] "Effect of neutron irradiation on laser diode properties", C. Barnes, D. Heflinger and R. Reel, SPIE Vol. 1174 "Fiber Optics Reliability: Benign and Adverse Environments III", p. 233 (1989).

[8] "5.5-MeV proton irradiation of a strained quantum-well laser diode and a multiple quantum-well broad-band LED", B. D. Evans, H. E. Hager and B. W. Hughlock, IEEE Trans. Nucl. Sci., Vol. 40, No. 6, p. 1645 (1993).

[9] "Space-radiation effects on optoelectronic materials and components for a 1300nm fiber optic data bus", P. W. Marshall et al., IEEE Trans. Nucl. Sci., Vol. 39, No. 6, p. 1982 (1992).

[10] "Radiation effects in optoelectronic devices", H. Lischka et al., SPIE vol. 2425, p.43, (1994).

[11] "SCH laser recombination rate from EBIC profiles", M. J. Romero, D. Araújo and R. García, Mat. Sci. and Eng. B42 p.172 (1996).

[12] Several different methods can be used to determine the threshold current, slope-efficiency and non-linearity. Some of these are outlined in "Reliability Assurance for loop optoelectronic. Special procedures and test methods for lasers", TA-NWT-000983, Issue 2, December 1993. Bellcore, Morristown, NJ 07960-06438, USA.

[13] "CMS tracker optical readout link specification. Draft version 0.5", F. Vasey CERN ECP/CME.

[14] "Beam test performance of the APV5 chip", M. D. M. de Fez-Laso et al., Nucl. Inst. and Meth., A 382, p. 533 (1996).

[15] "A neutron irradiation facility featuring cryogenic temperatures and dedicated to Large Hadron Collider detector design", J. Collot et al., Nucl. Inst. and Meth., A 350 (1994), p525.

[16] CMS Note in preparation.

[17] "Proton damage effects on light emitting diodes", R. H. Rose and C. E. Barnes, J. Appl. Phys., Vol. 53(3), p. 1772 (1982).

[18] "Gamma and neutron damage studies of optical fibres". K. Gill et al., to be published in J. Non-Cryst. Sol. (1997).

[19] P. Nugent and co-workers of Italtel, 20019 Settimo Milanese, Italy were responsible for the spectrum measurements.

[20] "Radiation damage by neutrons and photons to silicon detectors", K. Gill et al., Nucl. Inst. and Meth. A322 p.177 (1992).

[21] "Displacement damage in GaAs structures", G. P. Summers et al. IEEE Trans. Nucl. Sci. 35, No. 6, p. 1221 (1988).